PCCP

Proton NMR Relaxation from Molecular Dynamics: Intramolecular and Intermolecular Contributions in Water and Acetonitrile

Journal:	*Physical Chemistry Chemical Physics*
Manuscript ID	CP-ART-09-2019-004976.R2
Article Type:	Paper
Date Submitted by the Author:	20-Nov-2019
Complete List of Authors:	Philips, Adam; University at Buffalo, State University of New York, Chemistry Autschbach, Jochen; University at Buffalo, State University of New York, Chemistry

Proton NMR Relaxation from Molecular Dynamics: Intramolecular and Intermolecular Contributions in Water and Acetonitrile

Adam Philips, and Jochen Autschbach*

Department of Chemistry
University at Buffalo
State University of New York
Buffalo, NY 14260-3000, USA
email: jochena@buffalo.edu

Abstract: NMR relaxation rates for protons in liquid water and neat acetonitrile were computed based on ab initio molecular dynamics (aiMD) with forces from Kohn-Sham (KS) theory as well as force-field (FF) based classical dynamics. Intra- and intermolecular dipole-dipole contributions were separated, and nearly quantitative agreement with experiment was obtained for water. Spin-rotation (SR) contributions to the intramolecular relaxation rate in acetonitrile were computed using nuclear SR coupling tensors obtained from KS theory, and improved the total computed intramolecular rate to within a factor of two of experiment. Insufficient sampling of rare short-time collision events between neighboring acetonitrile molecules in the simulations is hypothesized as a major source of error in the intermolecular contributions.

1 Introduction

Magnetic dipole-dipole interactions mediated by molecular motion constitute the primary mechanism for ^{1}H relaxation in NMR spectroscopy. Relaxation data obtained from NMR experiments are an important source of information regarding the details of molecular motion for a chemical system. Interpreting the experimental results is nearly always accomplished via predefined motional models. To this end, much of the theoretical work in NMR relaxation theory has been devoted to development of these models,[1–6] which tend to be specific to a certain kind of system or set of conditions, assume an analytical form of the relevant time autocorrelation functions (ACFs), and sometimes require additional empirical data such as a radial distribution function (RDF) for the bulk system. While these models may work well, by their nature they ignore subtle details of dynamics at the molecular level and it is often difficult to know a priori if a given model is applicable to a particular system. For these reasons, it is important to study NMR relaxation phenomena via molecular dynamics (or Monte Carlo) simulations circumventing the need for empirical models. There are many sophisticated force fields available that can provide accurate trajectories in molecular dynamics for different classes of molecules. Inherent approximations notwithstanding, as it becomes computationally more tractable, a first principles approach to determine the forces in molecular dynamics is more general, as it does not require a force field that is parameterized a-priori and known to be suitable for the system of interest. It is therefore important to develop and

test first-principles theory tools for predicting relaxation phenomena,[7–11] in addition to utilizing force-field methods for the dynamics.

While proton NMR is ubiquitous in chemistry and elsewhere, much remains to be learned about the dynamic mechanisms that drive relaxation in even the simplest molecular systems. Previous work from our group[8–10] has focused on the quadrupolar interaction, which tends to dominate the relaxation for nuclei with spin quantum number I greater than 1/2. For $I = 1/2$ nuclei, which are not quadrupolar, the primary relaxation mechanism in diamagnetic systems is the dipole-dipole interaction. Dipolar relaxation, as the name implies, is driven by the fluctuating fields generated via the interaction between two nuclear magnetic dipoles. The interaction may take place intramolecular and intermolecular. The intramolecular portion is driven by nuclear vibrations and rotations within the molecule. The intermolecular contributions are primarily driven by translational diffusion[1] and more difficult to describe generally, arising when spin-half nuclei from neighboring molecules interact at a near enough distance to induce a fluctuating local field sufficient to cause relaxation. In general, the intermolecular interactions occur at a slower time scale than the intramolecular interactions, and it has even been suggested that the fast motion limit is inapplicable in this context,[12] even though the slow motion regime is usually only invoked for macromolecules such as proteins, or for very viscous fluids. It has also been demonstrated experimentally that intermolecular cross-relaxation effects such as between ^{1}H and ^{19}F result in relaxation associated with the slow motion regime.[13] However for indistinguishable nuclei in small molecule, non-viscous fluids, theory[14] and experiment[15] substantiate the fast-motion limit, where the spectral densities and therefore the relaxation rates are expected to be frequency independent.

There have been a number studies of dipolar NMR relaxation in simple molecular systems using classical force-field driven molecular dynamics (FFMD) in the past few decades.[11,12,14,16,17] For instance, Lippens et al.[14] used a single point charge (SPC) water model augmented with point polarizability[18] and reported very good agreement with experiment for intermolecular contributions, while underestimating the intramolecular contribution by nearly a factor of three. Calero et al.[11] explored several different classical water models and determined that the only model investigated which reproduced the experimental relaxation rate quantitatively was the TIP4P/2005 model. The team also considered a single, sub-20 ps Kohn-Sham (KS) density functional theory (DFT) based ab-initio MD (aiMD) simulation of the Car-Parrinello type. Westlund et al.[16] simulated neat acetonitrile using purely electrostatic and Lennard-Jones potentials and obtained the intermolecular relaxation rate within about 30% of the experimental value at the target temperature. Gerig[17] later studied acetonitrile as well, using a six-site interaction model,[19] resulting in intra- and intermolecular contributions computed to within about 25% of experiment. In a fundamental study conducted by Odelius et al.[12] utilizing simple Lennard-Jones particles, questions were raised as to the reliability of intermolecular results from simulations of insufficient length as

well as the validity of the extreme narrowing condition in this context. Further, in our previous aiMD work on quadrupolar relaxation in (heavy) water we showed variations between the relaxation data from different sub-20 ps trajectories, such that a more extensive sampling appeared necessary.

In the present work, we use FFMD and aiMD to compute ^{1}H dipolar relaxation rates in liquid water and acetonitrile and explore the dynamic mechanisms responsible for relaxation. Section 2 summarizes the theory and working equations for the computation of dipole-dipole driven relaxation rates from molecular dynamics, and provides computational details. Section 3 presents relaxation results for water and acetonitrile from aiMD and FFMD in comparison to experiment. We also make comparisons with a high level aiMD simulation for water performed by DiStasio et al.[20] and estimate the intermolecular contributions to the dipolar relaxation with RDF-based models of Harmon and Muller. Furthermore, the spin-rotation contributions to the relaxation rates are calculated and shown to improve the calculated relaxation rate for acetonitrile while being negligible for water. Section 4 provides general conclusions and an outlook.

2 Theoretical and Computational Details

The theoretical framework for nuclear spin relaxation was established by Bloembergen, Purcell, Pound[21] and Redfield.[22] A selection of specialized texts devoted to the topic includes the ones by Spiess,[23] Cowan,[24] and Kowalewski and Mäler.[25] The longitudinal relaxation rate, $1/T_1$ for a dipolar nucleus interacting with nuclei of the same type is given by[12,25]

$$\frac{1}{T_1} = \left(\frac{\mu_0}{4\pi}\right)^2 \gamma^4 \hbar^2 I(I+1)\left[J_1(\omega_0) + 4J_2(2\omega_0)\right] \tag{1}$$

Here, μ_0 is the permeability of free space, γ is the gyromagnetic ratio of the dipolar nucleus, I is the nuclear spin quantum number, and $J_m(\omega_0)$ are the spectral densities associated with the dipolar interaction at the Larmor frequency ω_0. The spectral density is defined via a half-Fourier transform of the ACF associated with the dipolar interaction,

$$J_m(\omega) = 2\,\mathrm{Re}\left[\int_0^\infty G_m(\tau) e^{-i\omega\tau} dt\right] \tag{2}$$

Further, $G_m(\tau)$ is the time ACF of the dipolar interaction and is denoted as

$$G_m(\tau) = \left\langle F_m^{ij}(t_0) F_m^{ij*}(t_0+\tau)\right\rangle \tag{3}$$

The brackets signify an ensemble average over all spin pairs i and j and time origins t_0. As in reference 17, $G(\tau)$ (without the index m) is taken to be the average of the $m = 1$ and $m = 2$ components of $G_m(\tau)$. The correlation time τ_c for the dipolar relaxation process can be defined via the following relation

$$\tau_c = \frac{1}{G(0)} \int_0^\infty G(\tau) d\tau \tag{4}$$

where $G(0)$ is the total variance of the dipolar interaction.

The interaction, $F_m^{ij}(t)$ between two dipolar nuclei whose motion drives the relaxation is defined as

$$F_m^{ij}(t) = \sqrt{\frac{4\pi}{5}} Y_{2,m}\left[\Omega_{ij}(t)\right] r_{ij}^{-3}(t) \tag{5}$$

Here, $Y_{2,m}\left[\Omega_{ij}(t)\right]$ is a spherical harmonic depending on the collective set Ω_{ij} of the polar and azimuthal angles of the vector between nucleus i and j relative to the laboratory coordinate system. Further, r_{ij} is the internuclear distance.

For small molecules in non-viscous fluids, nuclear motion is in the extreme narrowing limit ($\omega_0 \tau_c \ll 1$) and the spectral density is constant for frequencies reasonably lower than $1/\tau_c$. Equation (2) then reduces to an integration of the ACF, yielding the spectral density at zero frequency

$$J_m(0) = 2 \int_0^\infty G_m(\tau) d\tau \tag{6}$$

In this case, equation (1) can be rewritten by using $J_m(0)$ in place of $J_m(\omega_0)$.

Pioneering developments of models for nuclear spin relaxation by translational diffusion were made by Torrey.[1] Harmon and Muller (HM) extended Torrey's theory to include information provided by the radial distribution function of the liquid.[4] In Section 3, we invoke the HM model for the intermolecular spectral density, which is derived from a hybrid model of oscillatory molecular motion and diffusive jumps. As formulated by Sholl,[6] it is given by

$$J_1(0) = \frac{1}{20} \frac{8\pi n}{15\sigma D} \left[\frac{\sigma}{b} \left(5 - \frac{\sigma^2}{b^2} \right) + 5I_1 - 3I_2 \right] \tag{7}$$

where n is the spin number density in the system, D is the translational diffusion constant, σ is the distance of closest approach of molecules (defined by the first non-zero point on the center of mass RDF), and b is the distance at which the liquid loses structure (defined by the point at which the RDF converges to unity). The I_k, not to be confused with spin quantum numbers, are integrals

over the RDF, $g(r)$, defined by

$$I_k = \frac{1}{\sigma}\int_{\sigma}^{b}\left(\frac{\sigma}{r}\right)^{2k} g(r)dr\,, \quad k = 1,2 \tag{8}$$

The prefactor of 1/20 in equation (7) is different from the 1/30 in the paper of Sholl due to a slightly different (but equivalent) set of prefactors used in equations (1), (5), and the spherical harmonics. To obtain the intermolecular relaxation rate, the spectral density from equation (7) is substituted in Equation (1) with $J_1 = J_2$.

Car-Parrinello aiMD simulations (CPMD) of pure water and pure acetonitrile were carried out using the Quantum-Espresso (QE) software package.[26] Simulations of both systems utilized the exchange-correlation functional of Perdew, Burke, and Ernzerhof (PBE),[27,28] and additional simulations of water employed the revised PBE (revPBE) functional[29] based on a previous comparison between the functionals in water simulations.[30] For all simulations, we employed ultrasoft pseudopotentials from pslibrary1.0.0,[31] a kinetic energy cutoff of 100 Ry for the plane-wave (PW) basis, and a time step of 6.0 au (0.145 fs). For all PBE simulations, a fictitious electron mass (μ) of 380 au was used.[9,32,33] For revPBE simulations, a value of $\mu = 450$ au was found to be necessary for maintaining separation in the electronic and nuclear degrees of freedom. Water simulation cells contained 64 molecules. In order to keep the computational effort manageable, the acetonitrile simulation cells contained 32 solvent molecules. To yield simulations with densities equal to that of the liquid at ambient conditions, cubic cells with dimensions of 12.41 Å and 14.38 Å, respectively, were employed. Random initial cell packing and 5 ps of pre-equilibration with FFMD in the NVT ensemble was performed with the Tinker molecular modeling package[34] using the Optimized Potentials for Liquid Simulations all atom force field (OPLS-aa).[35] The aiMD simulations consisted of an additional 5 ps of equilibration in the NVT ensemble at 350 K using a three-chain Nosé-Hoover thermostat (90,45, and 15 THz), followed by dynamics in the microcanonical (NVE) ensemble. The first 1 ps in the NVE ensemble was also taken to be part of equilibration. For further comparison, sets of simulations with production fully in the NVT ensemble were explored. Production simulation times were 40-50 ps for long simulations and 25 ps for sets of short simulations. For acetonitrile, additional nanosecond time scale simulations at 300 K were performed entirely with FFMD in Tinker in both the NVT and NVE ensembles. Since classical dynamics allows for simulation of much larger systems, one of these simulations contained 500 molecules (cell dimension = 35.97 Å) and the intermolecular relaxation rate was computed according to equation 7. However, due to the computational scaling of the two-atom property calculations for the relaxation rates, and for better comparison with the aiMD results, only simulations containing 64 molecules (cell dimension = 18.13 Å) were used for computing relaxation rates via explicit cal-

culation and correlation of all dipole-dipole interactions. All FFMD simulations used a timestep of 1 fs. To ensure that the acetonitrile intermolecular forces were well approximated in our simulations, dimer binding energies were computed for cyclic and linear dimer configurations using the same DFT and FF levels of theory as utilized in the dynamics. These results are reported in the Supporting Information (SI) and follow the same trend as post-Hartree Fock calculations reported previously in the literature.[36] For all relaxation results reported in the main text, a cut-off radius of 23 au (12.17Å) was used for computing the dipole-dipole interactions at each snapshot. Convergence of the intermolecular relaxation rate with increasing cut-off distance was demonstrated for acetonitrile FFMD (See SI). Care was taken not to increase the cut-off distance larger than the simulation box dimension in order to avoid artifacts from periodic images.

As in previous work,[9,10,37,38] we corrected for the over-structured nature of water typically observed in aiMD simulations with non-hybrid functionals such as PBE[30,39] via an elevated simulation temperature of 350 K along with semi-empirical van der Waals corrections (D2) to the energies and forces.[40,41] When using revPBE, however, the system was simulated at the target experimental temperature of 300K with example simulations using both NVT and NVE ensembles for production. Dispersion corrections were still applied. It is unclear whether the elevated temperature discussed above is valid for ab initio acetonitrile in PBE. We ran PBE simulations at 300 and 350 K and the relaxation results are compared.

Post-processing of the MD trajectories including computation of two-atom distances corrected for periodicity, empirically determined bonding for separation of intra- and intermolecular pairs, RDFs, and trajectory visualization were accomplished using an open source tool developed in our group (version 0.4.1).[42] Code implementing the dipolar relaxation theory as defined in Section 2 was also written in-house using Python 3.

3 Results and Discussion

Tables 1 and 2 summarize the dipolar relaxation results computed from all performed simulations according to Equations (1) to (6). The experimental and computed longitudinal relaxation rates, along with the computed correlation time and total variance for the dipolar interaction are reported. Computed results are from each of our simulatiuons as well as an aiMD simulation by DiStasio et al.[20] Overall the calculated rates for water agree quite well with the experiment. The rates from the longest PBE simulation are in quantitative agreement with experiment, including the the values for intra- and intermolecular contributions when compared to the results reported by Goldammer and Zeidler.[44] In keeping with our previous work,[9,10] averages over several sets of independent trajectories were taken in order to get an idea of the statistical error in the calculations. Averages and standard errors are reported in Tables 1 and 2. According to these average total

relaxation rates, the 50 ps simulation yields results slightly outside the statistical range defined by the shorter trajectories. This may be an outlier or an indication that there is still some important correlation to be gained by sampling longer than 25 ps. A single 25 ps simulation utilizing revPBE slightly overestimated the relaxation rate, however it is within the range of the individual short

Table 1: Summary of dipolar ^{1}H NMR relaxation results[a] for water from various simulations.

	$\frac{1}{T_1}$	τ_c	$G(0)$	$\frac{1}{T_{1\,\mathrm{intra}}}$	$\frac{1}{T_{1\,\mathrm{inter}}}$
Exp.[43,44]	0.280	-	-	0.170	0.110
DiStasio (25ps)[20]	0.226	4.452	10.054	0.132	0.093
PBE,NVE (50 ps)	0.275	5.851	8.929	0.161	0.114
PBE,NVE 10×25 ps avg	0.229	4.972	9.110	0.140	0.094
PBE,NVE 10×25 ps err.	0.025	0.548	0.071	0.017	0.010
PBE,NVT 10×25 ps avg	0.130	2.824	9.049	0.078	0.052
PBE,NVT 10×25 ps err.	0.005	0.095	0.047	0.004	0.001
revPBE,NVT 10×25 ps avg	0.116	2.511	9.041	0.070	0.046
revPBE,NVT 10×25 ps err.	0.003	0.060	0.030	0.003	0.001
revPBE,NVE (25 ps)	0.340	7.752	9.308	0.199	0.141

[a] Data from current work except where noted otherwise. Calculations for our aiMD simulations used a sampling rate of every 300 frames (0.04 ps) and for the simulation of DiStasio the sampling rate was every 0.1 ps. Experimental values are extrapolated at 298 K from data in references 43 and 44 and are subject to their inherent experimental uncertainty. Relaxation rates are in Hz, τ_c is in ps, and $G(0)$ has units of $10^9 \mathrm{au}^{-6}$ where au is atomic units of distance or bohr. 'err.' indicates the standard error from averaging the results over ten independent simulations.

Table 2: Summary of dipolar ^{1}H NMR relaxation results[a] for acetonitrile from various simulations.

	$\frac{1}{T_1}$	τ_c	$G(0)$	$\frac{1}{T_{1\,\mathrm{intra}}}$	$\frac{1}{T_{1\,\mathrm{inter}}}$
Exp.[15]	0.067	-	-	0.046	0.020
PBE,NVE (350K,50 ps)	0.015	0.517	6.020	0.010	0.004
PBE,NVE (300K,40 ps)	0.023	0.731	5.943	0.017	0.006
PBE,NVE,350K 10×20 ps avg	0.018	0.578	5.961	0.013	0.005
PBE,NVE,350K 10×20 ps err.	0.001	0.022	0.029	0.001	0.000
FFMD (NVE,300K,1 ns)	0.033	1.050	6.303	0.024	0.009
FFMD (NVT,300K,1 ns)	0.032	0.987	6.311	0.022	0.009

[a] Data from current work except where noted otherwise. Calculations for the aiMD simulations used a sampling rate of every 300 frames (0.04 ps) and for the FFMD simulation the sampling rate was every 0.5 ps. Experimental values are extrapolated at 298 K from data in reference 15 and are subject to their inherent experimental uncertainty. Relaxation rates are in Hz, τ_c is in ps, and $G(0)$ has units of $10^9 \mathrm{au}^{-6}$ where au is atomic units of distance or bohr. 'err.' indicates the standard error from averaging the results over ten independent simulations.

PBE simulations, which are provided in the SI. We compare with a water simulation of DiStasio et al.[20] as well, for which the total relaxation rate falls within the range of rates from short PBE simulations with NVE.

Simulating with NVT systematically gives shorter correlation times and therefore lower rates. We tentatively attribute this finding to the thermostat influencing the thermal motion of the nuclei, which motivated us to perform the dynamics in the NVE ensemble in the first place. Namely, the relaxation mechanism is effective, with a high rate, when the fluctuating local fields de-correlate slowly. Apparently, the action of the thermostat causes an artificial de-correlation of the magnetic spin-spin interactions, leading to the lower calculated rates.

In the case of acetonitrile, the purely dipolar rate values in Table 2 systematically underestimate the experiment by at least a factor of 3 with aiMD. In the case of intramolecular relaxation, the underestimation in Table 2 is in part due to the exclusion of another fundamental mechanism of spin-rotation (SR) which is discussed at the end of this section. We decided to investigate FFMD simulations here in order to see if access to nanosecond scale simulation times improved the sampling for intermolecular contributions. Some improvement with respect to experiment is seen in the intermolecular and total relaxation rates. Due to the computational expense of the two-atom based correlation calculations, the length and sampling frequency used for these calculations is limited. As a result, the complete results reported in Table 2 are for the first 1 ns of the 2 ns simulations. To determine the necessary amount of sampling, several different sampling rates and total times were investigated (see SI). It was observed that the computed rate is somewhat sensitive to the sampling frequency used in the calculation but – beyond a certain limit – less so on the total sampled time.

Some insight into the structural contributions to proton relaxation in water and acetonitrile can be gained from the hydrogen-hydrogen RDFs. Figure 1 shows these RDFs, generated from the aiMD for both liquids, and compared to literature results.[45,46] In both cases there is a very sharp peak below 2 Å representing the intramolecular proton pairs (not seen in the purely intermolecular RDF from reference 46). The subsequent structure indicates intermolecular pairs, water expressing two resolved peaks due to the hydrogen bonding structure. Acetonitrile, however expresses a very broad intermolecular peak, at a somewhat greater average separation.[47–49] This is indicative of weaker ordering or pair correlation between protons on neighboring molecules. Because dipolar relaxation relies on the proximity and frequency of interacting spins in the system, this may explain the difficulty of obtaining accurate intermolecular ^{1}H NMR relaxation for acetonitrile in this study. This nature of the intermolecular interactions in acetonitrile is further evidenced by plotting the value of the dipolar interaction, $F_{2,m}(t)$ across a simulation as is done in Figure 2. $F_{2,0}$, as defined in equation (5), is plotted for a single representative proton pair on separate molecules for 1 ns of the FFMD acetonitrile simulation. It is seen that spikes in this quantity,

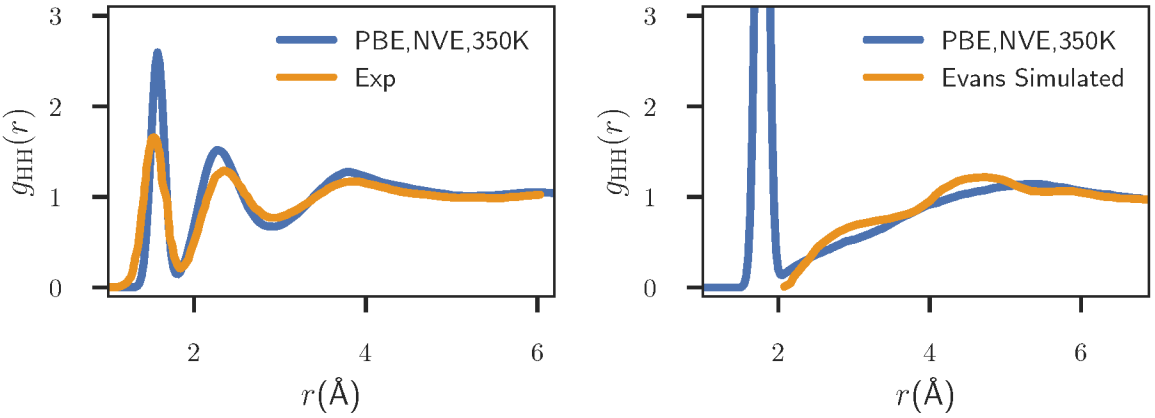

Figure 1: Hydrogen-hydrogen RDFs from 50 ps aiMD water, compared to experiment from reference 45 (left) and 50 ps aiMD acetonitrile, compared to a classical simulation from reference 46 (intermolecular only) (right)

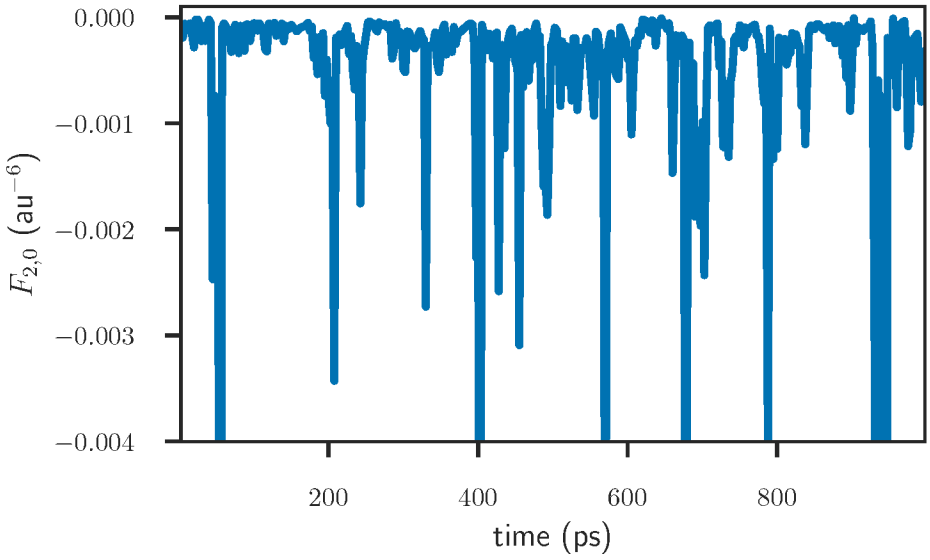

Figure 2: $F_{2,0}$ component of the dipolar interaction as defined in equation (5) for a representative pair of protons on different acetonitrile molecules across 1 ns of FFMD simulation.

which correspond to the spins getting sufficiently close to interact, are brief and relatively rare on the picosecond time scale. The rarity and transient nature of these collisions explains the necessity for extended sampling as well as the sensitivity of the relaxation results to sampling frequency.

Sholl determined the behavior of the intermolecular spectral density according to several models of translational diffusion and showed that, at the low frequency limit, the spectral density is

linear with the square root of the frequency.[6,12]

$$J(\omega) \cong J(0) - c\omega^{\frac{1}{2}} \tag{9}$$

As shown by Odelius et al.,[12] this relationship can be used to extrapolate the spectral density obtained from a molecular simulation to determine its value at zero frequency or at the Larmor frequency (ω_0 ranges from 20 to 25 MHz for protons in the fields produced by the spectrometers in the cited experimental works[15,43,44]). Figure 3 plots the $m = 1$ component of the spectral density for the intermolecular dipolar interaction from our 50 ps aiMD water simulation against the square root of the frequency. Linear extrapolation (dashed line) to the Larmor frequency and substitution into equation (1) yields an intermolecular rate of 0.073 Hz, a bit lower than the corresponding value reported in Table 1 obtained via direct integration of the ACF. Odelius et al. deemed the frequency dependence of the spectral density at low frequency described by equation (9) as fundamentally at odds with the extreme narrowing condition.[12] However in our case, taking the zero-frequency limit of the spectral density by integration of the ACF seems to give the best approximation of the experimental relaxation rate. Furthermore, as Odelius et al. pointed out, the extent to which the low frequency values of the spectral density can be calculated, is directly dependent on the length of simulation. Nanosecond scale FFMD simulations for acetonitrile allow extension of the intermolecular spectral density further into the low frequency region which is shown in Figure 4. The lack of a pronounced frequency dependence below ca. $5 \cdot 10^{-3}$ ps^{-1} is in fact consistent with the extreme narrowing condition.

As introduced in Section 2, Harmon and Muller developed a model for intermolecular dipolar relaxation, building on the theory of Torrey, but including information from the RDF. In their original formulation, and as implemented in the current work, this model assumes that all spins are at the center of spherical molecules. Therefore the RDFs used here are those of the centers of mass of molecules in the system. We invoke this method in order to assess the relaxation results as a function of the structure of the simulated liquids, as well as to remove the variables of sampling for the autocorrelation functions and of configurations which have a specific orientation as to drive the dipolar interaction. Table 3 summarizes our results from this model for each of our simulations, including the intermolecular relaxation rate itself, the diffusion coefficient D, and a parameter $I_{g(r)} = 5I_1 - 3I_2$ where I_k are integrals over the RDF as defined in equation (8). Again, our aiMD water simulations reproduce the experimental intermolecular rate quite well. Here, the simulation of DiStasio et al. which is known to reproduce the experimental water structure very well, gives a larger result for the relaxation rate, outside the range of standard error from our 25 ps PBE simulations and higher than the experiment. Comparisons of the oxygen-oxygen and hydrogen-hydrogen RDFs from our 50 ps PBE water simulation with those from DiStasio et al.

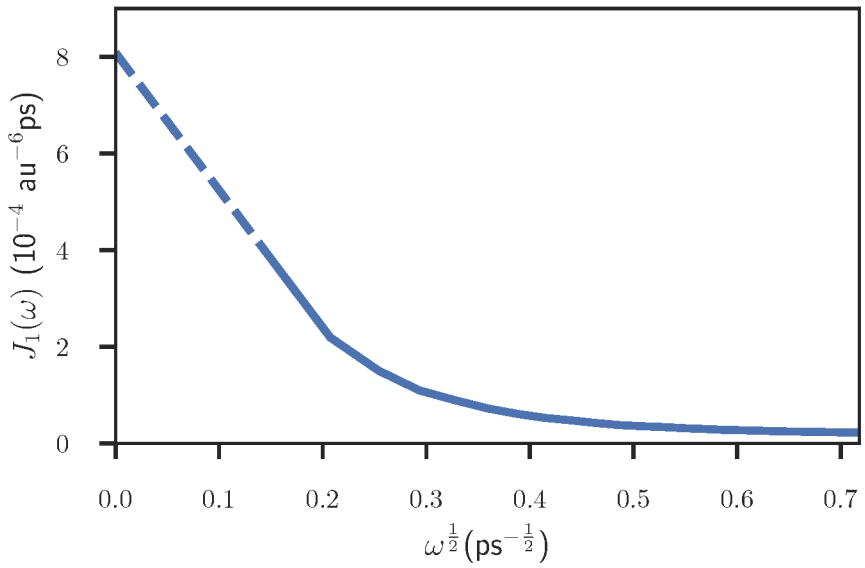

Figure 3: J_1 component of the intermolecular dipolar spectral density from a 50 ps aiMD water simulation. Generated via half-Fourier transform of the corresponding ACF. The result is plotted against the square root of frequency and a linear extrapolation in the low frequency region is shown as a dashed line. The proton Larmor frequency is taken to be 25 MHz (2.5×10^{-5} ps^{-1}) for the purposes of extrapolating with equation (9)

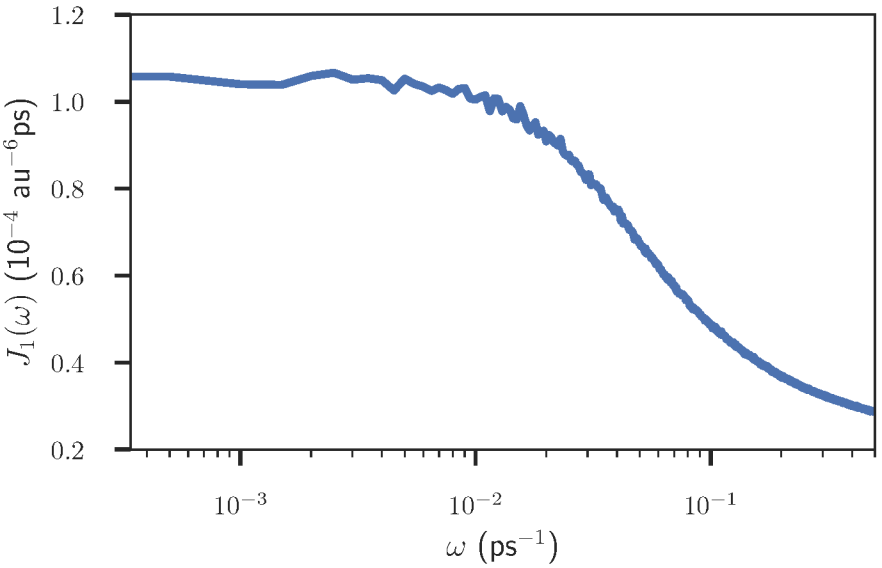

Figure 4: J_1 component of the intermolecular dipolar spectral density from a 2 ns FFMD acetonitrile simulation. Generated via half-Fourier transform of the corresponding ACF. The proton Larmor frequency is at 25 MHz (2.5×10^{-5} ps^{-1}) at the field strength used in the experiments by Woessner et al.[15]

and with experiment[45] are provided in Figure 5. The intermolecular structure is clearly softened with the use of a hybrid functional and explicit treatment of dispersion in the work of DiStasio et al. While there is certainly a possibility that the formally better simulation of DiStasio et al. exposes an underlying error cancellation in the PBE-based data, given the approximations leading to Equation (7), we are reluctant to draw a strong conclusion based on a single aiMD trajectory. The intermolecular relaxation rate for acetonitrile is improved with the Harmon-Muller model, compared to the results in Table 2, coming within a factor of 2 of the experimentally derived value. This may in part be attributed to the treatment of the centers of mass instead of the full molecular structure in which the spins are off center. This off-center structure along with relatively unstructured H-H pair correlation were discussed above as reasons for the underestimation from the full, dynamic theory. The center of mass treatment means that relative orientation of the spin carrying molecules does not play a role in facilitating interaction between neighboring spins, as they are treated simply as points. The relaxation model is also dependent on the translational diffusion constants which were also computed and are reported in table 3. For water, the computed diffusion constants agree with experiment very well,[50,52] especially given how difficult they have been shown to reproduce from aiMD.[53] For acetonitrile, reasonable agreement with the experimental diffusion constant is achieved from a ten trajectory average and by FFMD.

Table 3: Intermolecular ^{1}H NMR relaxation results[a] utilizing the RDF-based model of Harmon and Muller

	$\frac{1}{T_{1\,\mathrm{inter}}}$	D	$I_{g(r)}$
Water Exp.[44,50]	0.110	0.230	-
Water PBE,NVE (50ps)	0.139	0.162	2.534
Water PBE,NVE 10×25ps avg	0.134	0.202	2.547
Water PBE,NVE 10×25ps err.	0.022	0.026	0.001
Water revPBE,NVT 10×25ps avg	0.077	0.295	2.503
Water revPBE,NVT 10×25ps err.	0.004	0.013	0.001
Water DiStasio (25ps)	0.171	0.127	2.431
Acetonitrile Exp.[15,51]	0.020	0.318	-
Acetonitrile PBE,NVE (50ps)	0.010	0.806	1.809
Acetonitrile PBE,NVE 10×20ps avg	0.016	0.532	1.814
Acetonitrile PBE,NVE 10×20ps err.	0.001	0.030	0.003
Acetonitrile FFMD (NVE,2ns)	0.017	0.471	1.857

[a] RDFs are of the molecular centers of mass. The quantities σ and b in equation (7) are determined from the RDF and correspond to 2.3Å and 6.25Å for water and 2.75Å and 6.5Å for acetonitrile respectively. Acetonitrile FFMD with 500 molecules. The experimental diffusion constants are reported for the liquids at 298 K. The relaxation rate is in Hz, diffusion coefficient in Å^2/ps, and $I_{g(r)}$ is in Å^{-1} and is equal to $5I_1 - 3I_2$ with I_k as defined in equation (8).

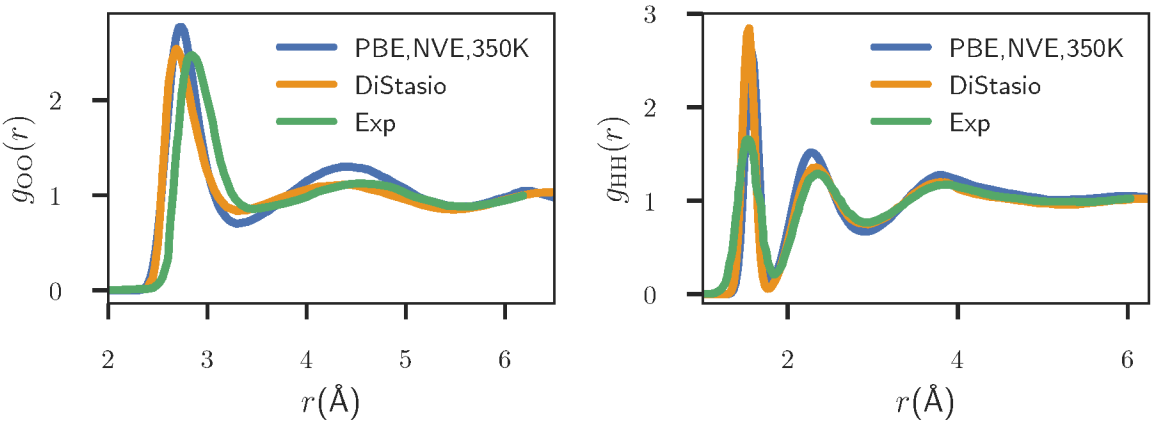

Figure 5: Oxygen-oxygen (left) and hydrogen-hydrogen (right) RDFs from our 50 ps aiMD water simulation, the simulation of DiStasio et al. (taken from reference 20), and the experiment from reference 45

We summarize our findings up to this point: Using the full dynamic approach defined by equations (1) through (6) in the extreme narrowing limit, accurate longitudinal ^{1}H relaxation rates with respect to experiment were obtained for water from KS-based aiMD with PBE and revPBE functionals. The high level hybrid-functional simulation of DiStasio et al. provided similar results to PBE at elevated temperature. Underestimation of ^{1}H relaxation in acetonitrile can be attributed to remaining limitations in the sampling, caused in part by weak H-H pair correlation. A nanosecond-scale classical MD simulation yielded an improved value for the total relaxation. The intermolecular spectral density plot from this FFMD simulation was found to be consistent with the extreme narrowing condition. The RDF-based methods of Harmon and Muller were also used to approximate the intermolecular contributions to dipolar relaxation rates. The model yielded slightly elevated intermolecular rates compared to the full dynamic approach, corresponding to an improvement with respect to experiment for acetonitrile. However, the spin rotation contributions to the relaxation still need to be determined (vide infra).

There are several fundamental sources of error that influence the relaxation results computed from MD. Firstly, sampling is finite in time as well as system size, given that the properties in question are measured on NMR time scales and on macroscopic samples. In addition, the approximations inherent in the forces computed in the dynamics, whether KS DFT or force-field based, impact the molecular trajectories and therefore the properties of the system. Lastly, nuclear quantum effects, which are not included here, may play a significant role in the dynamics that drive NMR relaxation for protons. Here and in the simulations by DiStasio et al., an elevated temperature is used as a crude approximation to mimic these effects. Further investigation with specialized aiMD methods implementing nuclear quantum effects is needed to determine their

importance.

It has been argued that the spin-rotation mechanism plays a significant role in the relaxation of acetonitrile protons.[15] This mechanism originates from the interaction of the spins with the magnetic field generated by rotation of the electronic charge in the molecule and is therefore an intramolecular contribution to the relaxation rate. For acetonitrile at ambient conditions, this mechanism and the dipole-dipole interaction are thought to contribute roughly equally to the intramolecular relaxation, and therefore the dipolar intramolecular relaxation rates collected in Table 2 must be corrected for this effect to be compared to the experimental measurements.

Woessner et al.[15] obtained intermolecular and intramolecular relaxation rates for aceetonitrile via isotope dilution experiments. Two opposite temperature dependencies for the intramolecular contribution to the relaxation rate were observed, characteristic of the coupled dipolar and SR mechanisms. The purely dipolar contribution, $(1/T_1)_{\mathrm{D}}$ was estimated using the following equation

$$\left(\frac{1}{T_1}\right)_{\mathrm{D}} = 3\gamma^4\hbar^2 b^{-6}\tau_{cp} \tag{10}$$

Here, γ is the proton magnetogyric ratio, b is the distance between two methyl protons (1.78Å), and τ_{cp} is an effective correlation time for the proton motion in the molecule based on quadrupolar relaxation measurements for ^{14}N and ^{2}D and rotational diffusion models for axially symmetric ellipsoids. The resulting dipolar contribution was substracted from the total intramolecular component to obtain the SR contribution. The value reported for the SR contribution at 298 K was 2.58×10^{-2} Hz.

In order to validate their results, Woessner et al. proceeded to compute the components of the nuclear SR coupling tensor, $C_\perp$ and $C_\parallel$, from their estimated rate, via the following equation:

$$\left(\frac{1}{T_1}\right)_{\mathrm{SR}} = \frac{1}{9}\frac{\Theta^2}{\hbar^2}(2C_\perp^2 + C_\parallel^2)\frac{1}{\tau_r} \tag{11}$$

This model assumes a spherical molecule with a single rotational correlation time, τ_r, and a corresponding moment of inertia, Θ. Since acetonitrile is not spherical, but rather a symmetric top, equation (11) can be invoked for rotation about the major and minor axes separately giving upper and lower bounds for the total SR relaxation rate. Using their empirically determined SR relaxation rate, Woessner et al. used this approach to obtain upper and lower bounds on the value of $2C_\perp^2 + C_\parallel^2$. Presumably due to lack of SR data acetonitrile in the literature, Woessner et al. compared the resulting values for $2C_\perp^2 + C_\parallel^2$ to experimental values for methane obtained by Rugheimer and Hubbard.[54] These experimental methane SR components correspond to $C_\perp = -111 \times 10^3$ Hz and $C_\parallel = 23 \times 10^3$ Hz. Woessner et al. found their estimated upper and lower limits to bound the

cited experimental values.

The SR tensor can also be computed ab initio at the KS DFT level of theory, for example as implemented in the Dalton suite of programs.[55,56] Accordingly, we calculated the SR tensor for acetonitrile with the B3LYP hybrid functional and the IGLO-III basis.[57,58] The results converted to the appropriate units are $C_\perp = 100\times10^3$ Hz and $C_\parallel = 3.02\times10^3$ Hz. The rotational correlation times for rotation about the major ($\tau_\parallel$) and minor ($\tau_\perp$) axes of acetonitrile were calculated from our simulations which yielded $\tau_\parallel = 0.28$ ps ($\Theta_\parallel = 5.441 \times 10^{-40}$ g cm^2) and $\tau_\perp = 1.55$ ps ($\Theta_\perp = 91.11 \times 10^{-40}$ g cm^2). Substitution in equation (11) yields upper and lower bounds on the SR contribution to the intramolecular relaxation rate. Using the SR coupling data of Rugheimer and Hubbard, a range of 2.66×10^{-3} to 1.34×10^{-1} Hz is obtained, while using the results of the ab initio SR calculations for the acetonitrile molecule, a range of 2.12×10^{-3} to 1.07×10^{-1} Hz is obtained. The SR rate estimated by Woessner et al. for 298 K is 2.58×10^{-2} Hz. When the SR contribution to the intramolecular relaxation rate, based on the calculated SR tensor, is combined with the dipolar contribution calculated from our aiMD simulations, a range of 1.2×10^{-2} to 11.7×10^{-2} Hz is obtained. This range brackets the experimental value of 4.6×10^{-2} Hz and indicates that for acetonitrile the intermolecular relaxation indeed has an important contribution from the SR mechanism due to the rotation about the major axis.

Liquid water, on the other hand, is not expected to experience a significant spin-rotation contribution near room temperature,[59] mainly due to a smaller rotational moment of inertia and slower molecular reorientation. Our calculations confirm this. A rotational correlation time of about 4 ps, extracted from the simulations, when combined with a KS DFT computation of the spin-rotation tensor, gives a spin-rotation contribution to the relaxation rate on the order of 10^{-5} Hz. Further details are provided in the SI.

4 Summary, Conclusions, and Outlook

^{1}H NMR relaxation rates in water and acetonitrile were computed from aiMD and FFMD simulations. The dipole-dipole driven relaxation was separated into intra- and intermolecular contributions which, for PBE water, agree nearly quantitatively with isotope dilution experiments. Approximations of the intermolecular relaxation rate via the RDF models of Harmon and Muller suggest that the structure of our simulated ab initio water is not worse than the structure from high level simulations of DiStasio et al. for the purpose of determining dipolar NMR relaxation, despite the weaker H–H structure in the latter.

Using nuclear spin-rotation coupling constants obtained from KS DFT, corrections for the spin-rotation contribution to acetonitrile intramolecular relaxation were made. With these corrections, the computed lower and upper bounds of the intramolecular relaxation for acetonitrile

bracket the experimentally derived value. The intermolecular contribution for acetonitrile apears to be systematically underestimated from our shorter simulations, but sampling from a nanosecond scale FFMD simulation improved the result to within approximately half of the experimentally reported value. The remainder is assigned to the SR mechanism. The extended simulation time of the FFMD also provided insight into the behavior of the intermolecular spectral density at low frequency, which displayed a lack of a frequency dependence consistent with the fast motion or extreme narrowing limit. These factors, along with the H-H RDF and plots of the dipolar interaction between protons on neighboring molecules, suggest that it remains challenging to obtain the necessary sampling of close intermolecular contacts, which drive this component of the relaxation, from practically achievable simulations for weakly structured liquids such as acetonitrile.

Our group continues to investigate quadrupolar and dipolar relaxation from high level aiMD simulation. Work is currently under way for several systems including Cs^+ in aqueous solution. ^{133}Cs has a comparatively small quadrupole moment and therefore may experience a non-negligible dipolar contribution in addition to the quadrupolar relaxation. We also aim to assess the impact of quantum nuclear effects on the proton relaxation in water.

Acknowledgments

We acknowledge the Center for Computational Research[60] at the University at Buffalo for providing computational resources, in particular those made available via grant MRI-1724891 from the National Science Foundation. We thank Dr. Robert A. DiStasio for providing a water trajectory. This work has been supported by grant CHE-1560881 from the National Science Foundation.

Suppplementary Information

Relaxation results for all individual short simulations of water and acetonitrile. Acetonitrile ^1H relaxation data from FFMD sampled at different lengths and frequencies. Computed acetonitrile dimer binding energies. Total energy plotted for FFMD, NVT versus NVE. Convergence of intermolecular relaxation rate with cut-off distance. Computed spin-rotation parameters and relaxation contribution for water.

References

[1] H. Torrey, *Phys. Rev.*, 1953, **92**, 962–969.

[2] P. S. Hubbard, *Phys. Rev.*, 1963, **131**, 275–282.

[3] B. Muller, *Can. J. Phys.*, 1966, **44**, 2511–2513.

[4] J. Harmon and B. Muller, *Phys. Rev.*, 1969, **182**, 400–410.

[5] R. McClung, *J. Chem. Phys.*, 1969, **51**, 3842–3852.

[6] C. Sholl, *J. Phys. C: Solid State Phys.*, 1981, **14**, 447–464.

[7] J. Schmidt, J. Hutter, H.-W. Spiess and D. Sebastiani, *ChemPhysChem*, 2008, **9**, 2313–2316.

[8] S. Badu, L. A. Truflandier and J. Autschbach, *J. Chem. Theory Comput.*, 2013, **9**, 4074–4086.

[9] A. Philips, A. Marchenko, L. A. Truflandier and J. Autschbach, *J. Chem. Theory Comput.*, 2017, **13**, 4397–4409.

[10] A. Philips, A. Marchenko, L. C. Ducati and J. Autschbach, *J. Chem. Theory Comput.*, 2019, **15**, 509–519.

[11] C. Calero, J. Martí and E. Guàrdia, *J. Phys. Chem. B*, 2015, **119**, 1966–1973.

[12] M. Odelius, A. Laaksonen, M. Levitt and J. Kowalewski, *J. Mag. Res.*, 1993, **105**, 289–294.

[13] L. Nordstierna, P. V. Yushmanov and I. Furó, *J. Chem. Phys.*, 2006, **125**, 074704.

[14] G. Lippens, D. Van Belle, S. Wodak and J. Jeener, *Mol. Phys.*, 1993, **80**, 1469–1484.

[15] D. Woessner, B. Snowden Jr. and E. Thomas Strom, *Mol. Phys.*, 1968, **14**, 265–273.

[16] P.-O. Westlund and R. Lynden-Bell, *J. Mag. Res.*, 1987, **72**, 522–531.

[17] J. Gerig, *Mol. Simulat.*, 2012, **38**, 1085–1093.

[18] A. Peter, W. Anders, E. Sven and B. Jönsson, *Mol. Phys.*, 1989, **68**, 563–581.

[19] A. M. Nikitin and A. P. Lyubartsev, *J. Comp. Chem.*, 2007, **28**, 2020–2026.

[20] R. A. DiStasio Jr., B. Santra, Z. Li, X. Wu and R. Car, *J. Chem. Phys.*, 2014, **141**, 84502.

[21] N. Bloembergen, E. Purcell and R. Pound, *Phys. Rev.*, 1948, **73**, 679–715.

[22] A. G. Redfield, *IBM J. Res. Develop.*, 1957, **1**, 19–31.

[23] H. W. Spiess, in *NMR Basic Principles and Progress*, ed. R. K. P. Diehl, E. Fluck, Springer, Berlin, 1978, vol. 15, pp. 55–214.

[24] B. Cowan, *Nuclear Magnetic Resonance and Relaxation*, Cambridge University Press, Cambridge, UK, 2005.

[25] J. Kowalewski and L. Mäler, *Nuclear spin relaxation in liquids: Theory, experiments, and applications*, Taylor & Francis, New York, 2006.

[26] P. Giannozzi, S. Baroni, N. Bonini, M. Calandra, R. Car, C. Cavazzoni, D. Ceresoli, G. L. Chiarotti, M. Cococcioni, I. Dabo, A. D. Corso, S. de Gironcoli, S. Fabris, G. Fratesi, R. Gebauer, U. Gerstmann, C. Gougoussis, A. Kokalj, M. Lazzeri, L. Martin-Samos, N. Marzari, F. Mauri, R. Mazzarello, S. Paolini, A. Pasquarello, L. Paulatto, C. Sbraccia, S. Scandolo, G. Sclauzero, A. P. Seitsonen, A. Smogunov, P. Umari and R. M. Wentzcovitch, *J. Phys. Cond. Mat.*, 2009, **21**, 395502.

[27] J. P. Perdew, K. Burke and M. Ernzerhof, *Phys. Rev. Lett.*, 1996, **77**, 3865–3868.

[28] J. P. Perdew, K. Burke and M. Ernzerhof, *Phys. Rev. Lett.*, 1998, **80**, 891.

[29] Y. Zhang and W. Yang, *Phys. Rev. Lett.*, 1998, **80**, 890.

[30] I.-C. Lin, A. P. Seitsonen, I. Tavernelli and U. Rothlisberger, *J. Chem. Theory Comput.*, 2012, **8**, 3902–3910.

[31] A. Dal Corso, *Comput. Mater. Sci.*, 2014, **95**, 337–350.

[32] J. C. Grossman, E. Schwegler, E. W. Draeger, F. Gygi and G. Galli, *J. Chem. Phys.*, 2004, **120**, 300–11.

[33] E. Schwegler, J. C. Grossman, F. Gygi and G. Galli, *J. Chem. Phys.*, 2004, **121**, 5400–5409.

[34] TINKER - Software Tools for Molecular Design by J. W. Ponder. URL `https://dasher.wustl.edu/tinker/`. Accessed 09/18.

[35] W. L. Jorgensen, D. S. Maxwell and J. Tirado-Rives, *J. Am. Chem. Soc.*, 1996, **118**, 11225–11236.

[36] J. R. Reimers and L. E. Hall, *J. Am. Chem. Soc.*, 1999, **121**, 3730–3744.

[37] L. C. Ducati, A. Marchenko and J. Autschbach, *Inorg. Chem.*, 2016, **55**, 12011–12023.

[38] L. Marchenko, A. Truflandier and J. Autschbach, *Inorg. Chem.*, 2017, **56**, 7384–7396.

[39] P. H.-L. Sit and N. Marzari, *J. Chem. Phys.*, 2005, **122**, .

[40] S. Grimme, *J. Comput. Chem.*, 2004, **25**, 1463–1473.

[41] S. Grimme, J. Antony, S. Ehrlich and H. Krieg, *J. Chem. Phys.*, 2010, **132**, 154104.

[42] T. J. Duignan and A. Marchenko, *Exatomic: A unified platform for computational chemists*, `https://github.com/exa-analytics/exatomic`, doi:10.5281/zenodo.60053.

[43] K. Krynicki, *Physica*, 1966, **32**, 167–178.

[44] E. V. Goldammer and M. D. Zeidler, *Ber. Bunsenges. Phys. Chem.*, 1969, **73**, 4–15.

[45] A. Soper, *Chem. Phys.*, 2000, **258**, 121–137.

[46] M. Evans, *J. Mol. Liq.*, 1983, **25**, 149–175.

[47] C. Hsu and D. Chandler, *Mol. Phys.*, 1978, **36**, 215–224.

[48] T. Takamuku, M. Tabata, A. Yamaguchi, J. Nishimoto, M. Kumamoto, H. Wakita and T. Yamaguchi, *J. Phys. Chem. B*, 1998, **102**, 8880–8888.

[49] M. Evans and G. Evans, *Adv. Chem. Phys.*, 2007, **63**, 377–491.

[50] A. J. Easteal, W. E. Price and L. A. Woolf, *J. Chem. Soc., Faraday Trans. 1*, 1989, **85**, 1091–1097.

[51] M. Afzal Awan and J. H. Dymond, *International Journal of Thermophysics*, 2001, **22**, 679–700.

[52] M. Holz, S. R. Heil and A. Sacco, *Phys. Chem. Chem. Phys.*, 2000, **2**, 4740–4742.

[53] H. S. Lee and M. E. Tuckerman, *J. Chem. Phys.*, 2007, **126**, 164501–16.

[54] J. H. Rugheimer and P. S. Hubbard, *J. Chem. Phys.*, 1963, **39**, 552–564.

[55] J. Gauss, K. Ruud and T. Helgaker, *J. Chem. Phys.*, 1996, **105**, 2804.

[56] S. P. A. Sauer, *J. Chem. Phys.*, 2010, **133**, 171101.

[57] W. Kutzelnigg, U. Fleischer and M. Schindler, in *NMR Basic Principles and Progress*, ed. P. Diehl, E. Fluck, H. Gunther, R. Kosfeld and J. Seelig, Springer-Verlag, Heidelberg, Germany, 1990, vol. 23, pp. 165–262.

[58] K. L. Schuchardt, B. T. Didier, T. Elsethagen, L. Sun, V. Gurumoorthi, J. Chase, J. Li, and T. L. Windus, *J. Chem. Inf. Model.*, 2007, **47**, 1045–1052.

[59] D. Smith and J. Powles, *Mol. Phys.*, 1966, **10**, 451–463.

[60] Center for Computational Research, University at Buffalo. URL `http://hdl.handle.net/10477/79221`. Accessed 08/29/2019.